THE JOURNAL OF BIOLOGICAL CHEMISTRY
Vol. 276, No. 33, Issue of August 17, pp. 31156–31162, 2001
Printed in U.S.A.

Structural Analyses of a Malate Dehydrogenase with a Variable Active Site*

Received for publication, January 31, 2001, and in revised form, May 31, 2001
Published, JBC Papers in Press, June 1, 2001, DOI 10.1074/jbc.M100902200

Jessica K. Bell‡, Hemant P. Yennawar§, S. Kirk Wright¶‖, James R. Thompson‡, Ronald E. Viola¶, and Leonard J. Banaszak‡ ‡‡**

From the ‡Department of Biochemistry, Molecular Biology and Biophysics, University of Minnesota, Minneapolis, Minnesota 55455, the §Department of Biochemistry and Molecular Biology, Pennsylvania State University, University Park, Pennsylvania 16802, and the ¶Department of Chemistry, University of Toledo, Toledo, Ohio 43606

Malate dehydrogenase specifically oxidizes malate to oxaloacetate. The specificity arises from three arginines in the active site pocket that coordinate the carboxyl groups of the substrate and stabilize the newly forming hydroxyl/keto group during catalysis. Here, the role of Arg-153 in distinguishing substrate specificity is examined by the mutant R153C. The x-ray structure of the NAD binary complex at 2.1 Å reveals two sulfate ions bound in the closed form of the active site. The sulfate that occupies the substrate binding site has been translated ~2 Å toward the opening of the active site cavity. Its new location suggests that the low catalytic turnover observed in the R153C mutant may be due to misalignment of the hydroxyl or ketone group of the substrate with the appropriate catalytic residues. In the NAD·pyruvate ternary complex, the monocarboxylic inhibitor is bound in the open conformation of the active site. The pyruvate is coordinated not by the active site arginines, but through weak hydrogen bonds to the amide backbone. Energy minimized molecular models of unnatural analogues of R153C (Wright, S. K., and Viola, R. E. (2001) *J. Biol. Chem.* 276, 31151–31155) reveal that the regenerated amino and amido side chains can form favorable hydrogen-bonding interactions with the substrate, although a return to native enzymatic activity is not observed. The low activity of the modified R153C enzymes suggests that precise positioning of the guanidino side chain is essential for optimal orientation of the substrate.

Malate dehydrogenase (MDH)[1] catalyzes the reversible oxidation of malate to oxaloacetate with the concomitant reduction of NAD or, in chloroplasts, NADP. The reaction is part of the citric acid cycle and, in eukaryotes, the malate/aspartate shuttle. MDH is highly selective for its 4-carbon dicarboxylic acid substrate, distinguishing malate from the readily available 3-carbon (pyruvate) and 5-carbon (α-ketoglutarate) mono- and di-carboxylic substrate analogues.

Insights into the substrate binding come from the crystallographic structures of eMDH·citrate·NAD complex (1), where citrate mimics the substrate, and cytoplasmic porcine MDH (cytMDH)·α-ketomalonate·tetrahydro-nicotinamide adenine dinucleotide (oxidized form) (2), in which α-ketomalonate is a substrate analogue. Both of these substrate mimics are coordinated by three arginine residues in the active site (Fig. 1). Two of these arginines, Arg-81 and Arg-87,[2] are located on a loop that bends into the active site and form hydrogen bond interactions with the 4-carboxyl and 2-hydroxyl/ketone of the substrate. A third arginine, Arg-153, completes the coordination of the substrate by hydrogen bonding to the 1-carboxyl group of the substrate. A histidine/aspartate pair, His-177 and Asp-150, present in all 2-hydroxyacid dehydrogenases (3), acts as a proton relay system during catalysis and requires correct positioning with the 2-hydroxyl group. The rather large anion pocket, which comprises the active site, can accommodate the 6-carbon moiety, citrate, and small negatively charged anions such as sulfate, suggesting that the coordination of the true substrate to target residues within the active site produces the specificity of the enzyme.

MDH and LDH, both 2-hydroxy-acid dehydrogenases, share similar tertiary structure and conservation of the nucleotide binding domain and catalytic residues, yet select for di- *versus* monocarboxylic acid substrates.

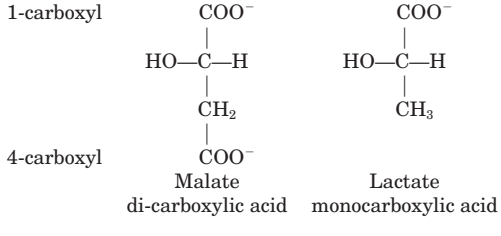

Chapman *et al.* (2) proposed that MDH is unable to bind the monocarboxylic acids with high affinity due to the charge repulsion that would occur between the two positively charged

* This work was funded by National Science Foundation Grants MCB9318699 (to L. J. B.) and MCB0196103 (to R. E. V.). The costs of publication of this article were defrayed in part by the payment of page charges. This article must therefore be hereby marked "*advertisement*" in accordance with 18 U.S.C. Section 1734 solely to indicate this fact.

The atomic coordinates and structure factors (code 1IE3 and 1IB6) have been deposited in the Protein Data Bank, Research Collaboratory for Structural Bioinformatics, Rutgers University, New Brunswick, NJ (http://www.rcsb.org/).

‖ Current address: Dept. of Biochemistry, University of Wisconsin, Madison, WI 53705.

** To whom correspondence may be addressed: Dept. of Chemistry, University of Toledo, 2801 W. Bancroft St., Toledo, OH 43606. Tel.: 419-530-1582; Fax: 419-530-1583; E-mail: ron.viola@utoledo.edu.

‡‡ To whom correspondence may be addressed: Dept. of Biochemistry, Molecular Biology and Biophysics, 6-155 Jackson Hall, 321 Church St. S.E., Minneapolis, MN 55455. Tel.: 612-626-6597; Fax: 612-626-2163; E-mail: len_b@dcmir.med.umn.edu.

[1] The abbreviations used are: MDH, malate dehydrogenase; NCS, non-crystallographic symmetry; cytMDH, cytoplasmic porcine malate dehydrogenase; eMDH, *E. coli* malate dehydrogenase; LDH, lactate dehydrogenase; a.s.u., asymmetric unit; CNS, Crystallography and NMR Systems software package; OAA, oxaloacetate; EAm, ethylamine; PAm, propylamine; PAd, propylamide; AAd, acetamide; AAn, acetamidine; Ac, acetate.

[2] For consistency all residues will be identified using the *E. coli* MDH numbering.

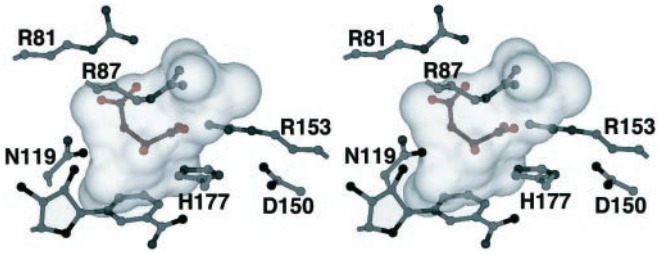

FIG. 1. **Stereoview of the MDH anion binding active site region.** The active site of MDH is formed by Arg-81, Arg-87, Asn-119, Asp-150, and His-177 (amino acids shown in *single-letter code* on figure). The *theoretical* model of malate (*1cme*) is shown in *red* and depicts what interactions may be occurring when substrate is bound. The transparent surface represents anions and substrate analogues that have been crystallized with MDH omitting sulfate B of the R153C·NAD structure for clarity. Anions were taken from *4mdh*, *5mdh*, *1emd*, and the two current structures. The large volume in which anions are able to bind exceeds the volume of the substrate itself. To increase catalytic efficiency, the enzyme appears to have targeted the substrate to the catalytic residues with the placement of arginine residues to coordinate and orient the negatively charged substrate within the active site. The interaction of Arg-87 with the anion surface occurs when pyruvate is bound and this residue is then swung out of the anion pocket. Similarly, NAD interacts with the anion surface when citrate is bound; in the crystal structure, the nicotinamide ring has rotated away from the pocket to accommodate citrate.

groups, Arg-81 and Arg-87, when the active site loop bends into the anion pocket. The binding of the dicarboxylic acid substrate to MDH is far more favorable for the two positive charges present as Arg-81 and Arg-87. LDH avoids this charge imbalance with a conserved glutamine at position 81. Manipulation of MDH and LDH specificity has been directed at point mutations of position 81 to Gln and Arg, respectively. In the LDH mutant, Q81R (4), substrate specificity was reversed from mono- to dicarboxylic acids. The R81Q MDH mutant exhibited no corresponding reversal of substrate specificity, only a broadened recognition of substrates with a marked reduction in overall catalytic rate. (5). The R81Q MDH indicated that specificity for malate/oxaloacetate could not be assigned to only one residue in the active site.

Structural analysis of a point mutant to manipulate substrate specificity is the basis of the current study. Wright and Viola (6) have mutated Arg-153 to a cysteine to disrupt the interaction with the 1-carboxyl group of malate during the catalytic reaction. Unexpectedly, the K_m of the enzyme for the substrate was essentially unchanged but catalysis was dramatically altered with k_{cat} for the interconversion of malate to oxaloacetate significantly decreased. In addition, R153C was shown to display increased capacity to utilize pyruvate as a substrate (6). Here we present crystal structures of the R153C·NAD binary complex and the R153C·NAD·pyruvate ternary complex. In addition, hypothetical energy-refined models have been determined for the interaction of the substrate with the chemical modifications that have been introduced at position Sγ of Cys-153.

EXPERIMENTAL PROCEDURES

NAD Complex—E. coli R153C MDH was expressed and purified as described by Hall *et al.* (7). Crystals were grown by the hanging drop vapor diffusion method out of a solution of 0.1 M Tris-maleate, pH 6.0, 24–30% polyethylene glycol 3350, 0.2 M ammonium sulfate. Crystals appeared in 7–10 days when grown at 18 °C. They were soaked in mother liquor plus 10 μM NAD for 1 h before mounting in a glass capillary.

Diffraction data were collected at room temperature on an R-AXIS IV^{2+} Rigaku imaging plate (Molecular Structure Corp. (MSC)). The diffraction data were indexed using the CrystalClear Software (MSC) into a C2 space group, with cell dimensions of a = 148.14 Å, b = 53.08 Å, c = 164.29 Å, and β = 95.26°. The phase information was obtained by using molecular replacement methods with AMoRe-CCP4 (an Automated package for Molecular Replacement; Ref. 8), and the native eMDH coordinates (1) as a probe. Four subunits (A through D) were placed in the a.s.u. Rigid body refinement was done with AMoRe-CCP4 (9). NCS "strict" constraints were used on one of the two dimers in the a.s.u. Model refinement was done with CNS version 0.5 (10). Initial rounds of refinement included simulated annealing, positional, and B factor refinement. The program O was used for model rebuilding after each round of refinement (11).

When the refinement reached an R_{cryst} of 0.25, ligands were placed in the model. The coordinates for NAD and SO_4^{2-} were downloaded from Heterocompound Information Center, Uppsala, Sweden (HIC-UP) (12). Positive electron density greater than 5 σ in an $|F_o| - |F_c|$ map was used for initial placement of heteroatoms. Solvent molecules were placed in the model using the water pick module of CNS. The criteria for placing solvent molecules were an $|F_o| - |F_c|$ peak $\geq 4\ \sigma$, a $2|F_o| - |F_c|$ peak ≥ 1, and good hydrogen bonding interactions with protein atoms. Placement of waters was verified by visual inspection. When the model reached an R_{cryst} of 0.23, NCS constraints were removed. The quality of the structure was assessed with both the WHATIF (13, 14) and PROCHECK (15) programs.

NAD·Pyruvate Complex—The R153C·NAD·pyruvate complex was formed in the presence of NAD (7 mM) and pyruvate (20 mM) and co-crystallized by hanging drop vapor diffusion out of a solution of 0.1 M sodium cacodylate, pH 6.5, 20% polyethylene glycol 4000, and 0.1 M ammonium acetate. Crystals (0.2 × 0.2 × 0.5 mm) grown at 24 °C were obtained 3 days after microseeding from a stock seed solution. The data on the ternary complex were collected at room temperature on an R-AXIS IV Rigaku image-plate detector (MSC) mounted on a RU200 rotating anode generator. The data were indexed into a C2 space group with unit cell parameters of a = 147.41 Å, b = 52.85 Å, c = 169.91 Å, and β = 101.76° and scaled using the HKL suite, DENZO, and SCALEPACK (16). Again, the structure was solved with the molecular replacement technique using the coordinates from *1emd* (1) as the probe and the software, AMoRe (8). The NCS matrices relating the four monomers were obtained from AMoRe and used as a strict restraint in the initial stages of the refinement. CNS version 0.9a (10) was used for refinement, map calculations, and placement of solvent molecules. The program O (11) was used for density visualization and modeling.

The density for NAD was identified, and the coordinates from the *1emd* structure matched the density well. Minor adjustments were done using O. Similarly, the pyruvate density was identified and the coordinates were obtained from the Uppsala Software Factory data base (12). After further refinement (R_{cryst} = 0.30), NCS constraints were removed and all four monomers were refined independently. The electron density for the pyruvate molecules among the four subunits in the a.s.u. was not consistent. In subunit C, the $2|F_o| - |F_c|$ density, contoured at 1 σ, could account for the entire molecule. In the remaining three subunits, electron density in the $2|F_o| - |F_c|$ map was either entirely missing or overlapped with only the 2-hydroxyl group of pyruvate. A simulated annealing omit map of each active site was employed to determine if pyruvate could be modeled into the three remaining subunits. The omit map did not indicate continuous density for pyruvate in subunits A, B, or D, so coordinates for the ligand were omitted.

The loop over the active site, residues 79–91, of each subunit was at least partially disordered. A composite omit map of the asymmetric unit was created to help interpret this area. Initially the occupancies for residues 79–91 of each subunit were set to zero. Starting from the two ends of the loop, residues were modeled into the electron density according to the omit and $|F_o| - |F_c|$ maps contoured at 1 σ. One to two residues were usually placed during each session of model rebuilding and then subjected to positional and B factor refinement. The placement of a residue was again evaluated by an $|F_o| - |F_c|$ map after each round of refinement. Of the four loops in the a.s.u., subunit B had the most contiguous electron density; only residue 87 was partially disordered. Subunits A, C, and D have residues 81–90, 80–86 and 83–86 disordered, respectively. Subsequently, the loop region for subunits A, C and D was modeled like subunit B with occupancies for disordered residues set to zero. The difficulties in modeling this region are reflected in the B factors, which average 85 $Å^2$ for residues 76–91 of subunits A, C and D.

Modeling the Chemical Modifications at R153C eMDH—The R153C·NAD structure was used as the basis for the cysteine modification models. Coordinates for the modified side chains that had been introduced (6) were first built onto the cysteine using the Biopolymer module of InsightII (Molecular Simulations Inc.). The modified cysteine side chain underwent one round of positional refinement in the Discover_3 module of InsightII using the minimize mode. The remainder of the molecule was fixed during refinement. The theoretical model of eMDH·NAD·malate (*1cme*) was superimposed onto the modified cys-

TABLE I
Data collection statistics

	NAD	NAD·pyruvate
X-ray wavelength	1.5418 Å	1.5418 Å
Crystallization conditions	0.1 M Tris-maleate, pH 6.0 24% polyethylene glycol 3350, 0.2 M $(NH_4)_2SO_4$	0.2 M Sodium cacodylate, pH 6.5 20% polyethylene glycol 4000, 0.1 M NH_4-acetate
Unit cell	a = 148.14 Å, b = 53.08 Å, c = 164.29 Å, β = 95.26 °	a = 147.41 Å, b = 52.85 Å, c = 169.91 Å, β = 101.76 °
Space group	C2	C2
Resolution	2.1 Å	2.5 Å
No. of reflections	201,844	95,846
No. of unique reflections	73,723	66,535
Completeness (last shell)	96.9% (84.8%)	87.5% (90.0%)
Subunit/a.s.u.	4	4
R_{merge} [a]	7.6%	11.5%
$I/\sigma I$	8.8	8.5
Redundancy	2.7	1.4

[a] $R_{merge} = (\Sigma|I_{hkl} - \langle I_{hkl}\rangle|/\Sigma I_{hkl}) \times 100$.

teine R153C model and the malate coordinates appended to the R153C modified cysteine model. The dihedral angles of the modified side chain were adjusted in Setor version 4.14.14 (17) to allow the most favorable position for hydrogen bonding interactions to the malate.

Figs. 1 and 5 were prepared using Setor (17). Figs. 2–4 were prepared using the software program SPOCK (by J. A. Christopher; available at quorum.tamu.edu/spock/). Figs. 2 and 4 are the product of a positive mask around the depicted atoms and the indicated electron density map.

RESULTS

NAD Complex—A summary of data collection statistics is given in Table I. The rotation and translation function studies initially placed one dimer in the asymmetric unit. Examination of the lattice packing clearly indicated the need for a second dimer that was subsequently placed using AMoRe. The Matthew's coefficient for two dimers in the asymmetric unit is 2.48 $Å^3$/Da. NCS "strict" averaging was used to constrain one of the two dimers in the a.s.u. during the initial rounds of refinement. With two dimers in the a.s.u., reference to individual subunits is done alphabetically for both x-ray studies. Therefore, in the coordinates and molecular images, the subunits are labeled A, B, C, and D.

Overall, the R153C·NAD structure is very similar to the wild type eMDH structure (1, 19) with a root mean square deviation between Cα atoms of 0.4 Å. The cofactor, as in the native eMDH structure, forms hydrogen bonds primarily to main chain atoms (1). The nicotinamide ring, in contrast to the Hall structure in which the cofactor may have been partially occluded from the active site by the carboxymethyl branch of the substrate analogue, citrate, has rotated about the nicotinamide glycosidic bond 57° farther into the active site. This ring movement was predicted in the theoretical model of eMDH·NAD·malate (*1cme*). The new orientation of the nicotinamide ring is stabilized by several hydrogen-bonding interactions: between the oxygen of the nicotinamide carboxamide to both the Nϵ2 of the catalytic histidine (177) and a solvent molecule and the nitrogen of the carboxamide to the carbonyl oxygen of Ile-117 (Fig. 2*A*).

The electron density for a portion of the active site in subunit B (residues 72–93) was poor and discontinuous. The occupancy for these residues was set to 0.5 and initially modeled by superimposing active site A onto active site B. Further modeling of active site B was then performed according to simulated annealing omit maps, $|F_o| - |F_c|$ maps and $2|F_o| - |F_c|$ maps contoured at 0.75 σ. Also absent from active site B was electron density for either the cofactor or sulfate ions; therefore, both ligands were omitted during modeling. A summary of the overall refinement statistics and model quality for the R153C·NAD complex is given in Table II.

In the R153C·NAD structure (Fig. 2*A*), the anion pocket is occupied by two sulfate ions (S-A and S-B) from the crystallization medium. Sulfate A binds in the catalytic region of the active site, which, in previous crystal structures (1, 2, 20), has been occupied by substrate analogues. The negative charges on the sulfate appears to be neutralized by hydrogen bonding and electrostatic interactions with the side chains of Arg-81, Arg-87, and Asn-119 and solvent molecules (Table III, Fig. 2). The position of sulfate A was compared with the cytMDH·NAD structure (20) in which only one sulfate is bound in the active site (Fig. 3). In cytMDH the sulfate ion interacts with the side chains of Arg-153, His-177, Ser-225 (Ala in *E. coli*), and Asn-119 (*E. coli* residue numbers, Table III). However, in R153C MDH, the loss of the guanidino group at position 153 results in sulfate A shifting 2 Å closer to the mouth of the active site and taking advantage of the charge neutralization provided by Arg-81 and Arg-87.

The second sulfate ion, labeled S-B, binds to the more solvent-exposed side of the loop and slightly away from the active site. This anion is hydrogen-bonded to the amide group of Gly-179 and the side chain of Arg-87. Together, the two sulfate ions create a seemingly effective mimic of the dicarboxylic substrate. By electrostatically coordinating both remaining arginine residues (Arg-81 and Arg-87), the sulfate ions bring the active site loop into the closed conformation (Fig. 3).

NAD·Pyruvate Complex—The structure of the ternary complex, R153C·NAD·pyruvate, has also been examined to determine the orientation of the 1-carboxylic acid substrate at the enzyme active site. A summary of the data collection statistics for this study is also given in Table I.

Electron density for pyruvate was identified in only one of the four subunits in the asymmetric unit of crystalline R153C MDH, and the results for this subunit are shown in Fig. 2*B*. Pyruvate is a monocarboxylic inhibitor of MDH and is bound in the active site without directly interacting with either Arg-81 or Arg-87. Instead, pyruvate forms rather long (3.6–3.85 Å) and potentially weak hydrogen-bonding interactions with the backbone amide groups of Gly-179, Gly-210, and Thr-211 and the solvent molecule, 478 (Table III). In the remaining subunits, the water structure is conserved with the overlap of a water molecule at the 2-hydroxyl position of pyruvate.

In this crystal structure, the four active site loops (residues 79–91) in the ternary complex are again partially disordered. Extensive model rebuilding using composite omit and $|F_o| - |F_c|$ maps was needed to define the position of this loop. Subunit B contained the most continuous electron density for this region, with only the side chain of Arg-87 appearing to be disordered. Atoms in this side chain were set at 0.5 occupancy. The undefined residues of this loop in subunits A, C and D have been modeled in the conformation of subunit B with zero occupancy for disordered residues. Complete refinement statistics are presented in Table II.

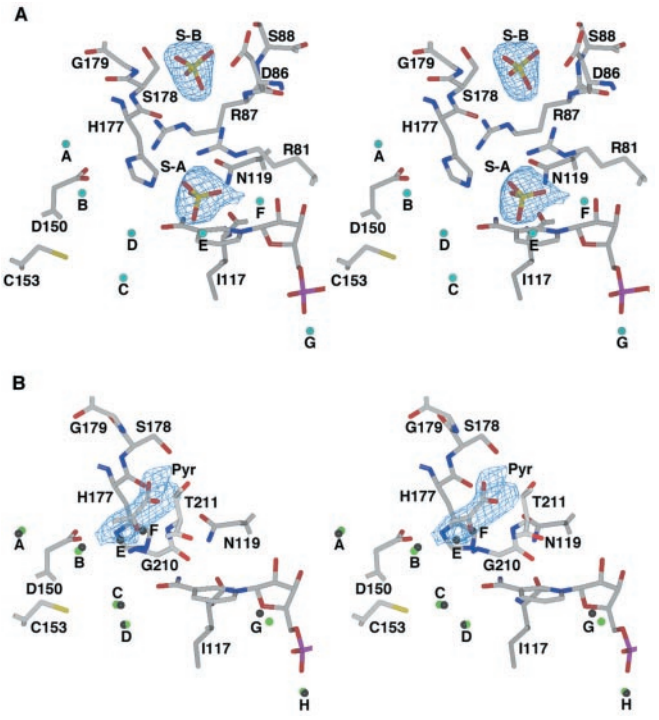

FIG. 2. **Stereo diagrams of the NAD and NAD·pyruvate active sites.** In both structures Cys-153 is no longer able to interact with anions or substrate bound in the active site and instead the sulfhydryl forms a hydrogen bond to a nearby water. *A*, the active site of R153C·NAD. A stereo diagram of the active site of subunit A with a 2.1Å $2|F_o| - |F_c|$ electron density map, contoured at 1 σ, enveloping the sulfate ions. The sulfate ions form hydrogen bonds to the guanidino groups of both Arg-81 and Arg-87, the amino group of Gly-179, Nϵ2 of His-177, and the Nδ1 of Asn-119. The nicotinamide ring position is stabilized by hydrogen bonds from the oxygen of the nicotinamide carboxamide to a solvent molecule and the Nϵ2 of the catalytic histidine (177) and the nitrogen of the carboxamide forms a hydrogen bond to the main chain oxygen of Ile-117. The binding site for sulfate A corresponds to the substrate binding site and maintains the same hydrogen bonding pattern. Sulfate B occupies a newly defined anion binding site. The majority of the hydrogen bonding interactions for this site arise from Arg-87. When substrate is bound, Arg-87 coordinates the 2-ketone/hydroxyl group during catalysis, but in the binary structure the closed loop may be stabilized by the second sulfate coordinating the positively charged Arg-87. *B*, the active site of R153C·NAD·pyruvate. A stereo diagram of the active site of subunit C, containing a bound pyruvate, superimposed with the water structure (*green spheres*) present in subunit B. Simulated annealing omit map density, contoured at 1 σ, depicts the placement of the pyruvate molecule. The pyruvate forms long and weak hydrogen bonds with the amino groups of residues Gly-179, Gly-210, and Thr-211. The lack of coordination by the remaining two arginines in the active site pocket (81 and 87) suggest that these residues are not necessary for ligand binding but for substrate orientation. Instead, in the open conformation, the main chain atoms lining the active site pocket may serve as an initial docking site for potential ligands.

TABLE II
Refinement statistics

	NAD	NAD·pyruvate
Resolution	2.1 Å	2.5 Å
R_{cryst}[a]	19.1%	18.4%
R_{free}[b]	24.5%	25.3%
Root mean square deviation bonds	0.014 Å	0.006 Å
Root mean square deviation angles	1.7 °	1.22 °
No. of atoms	9512	9423
Non-H protein atoms	9068	9068
Water	282	173
Ligand atoms		
NAD	132	176
SO_4^{2-}	30	
Pyruvate		6
Average B factor[c]	47.7	51.7
Protein	47.3	43.4
Main chain	45.0	41.3
Side chain	50.2	46.1
Water	48.6	42.8
Ligand[d]		
NAD	47.4	46.5
SO_4^{2-}	62.7	
Pyruvate		99.1
Ramachandran values[e]		
Most favored regions	90.9%	90.3%
Additional allowed regions	9.1%	9.7%
Generously allowed regions	0%	0%
Disallowed regions	0%	0%
Cis peptides	4	4

[a] $R_{cryst} = (\Sigma|F_o - F_c|/\Sigma|F_o|) \times 100$.
[b] The R_{free} set is 9.9% of the total reflections.
[c] The B factor statistics for the NAD·pyruvate structure excluded residues 79–91 for subunits A, C, and D.
[d] Occupancy varies from 0.5 to 1.0.
[e] Ramachandran values were derived from PROCHECK (15).

A striking difference exists between the active site loop of R153C MDH with bound coenzyme and pyruvate when compared with the NAD structure. The conformation of this loop, residues 79–91, and that of an adjacent loop, residues 214–221, are shown in Fig. 4*A*. Compared with the binary complex, residues 81–91 in the NAD·pyruvate structure have moved from as little as 1.5 Å to as much as 10.8 Å away from the active site to expose the anion/substrate binding pocket to solvent. This conformation resembles the open active site loop found in the cytMDH·NAD structure (Fig. 3).

The transition from the closed to open conformation involves a change in secondary structure for residues 86–90. The secondary structure was defined by the Kabsch and Sander method (21) in PROCHECK (15). In the closed conformation residues 86–89 form a bent 3_{10} helix with residue 90 beginning an α-helix, which extends to residue 108. Water molecules bridge the $i+4$ hydrogen bonding interactions at residues O92 to N96, O89 to N93 and O88 to N92, respectively, to accommodate the bending of the helix. In contrast, the open conformation forms an extended α-helix from residues 86 to 108. The extended helix does not bend into the active site. This, in turn, forces the remaining portion of the active site loop away from the anion-binding pocket. A second, smaller movement, occurs in the segment containing residues 214–221, which forms an opposing face to the active site loop in the closed conformation (Fig. 4*C*). When the active site loop moves to the open position, this adjacent loop shifts 1–3 Å. Fig. 4 shows the most apparent conformational differences between the open and closed mobile loop conformations.

Models of the Chemically Modified R153C eMDH—The new cysteine that was introduced at position 153 may be chemically modified to simulate arginine or lysine side chains. The modifications and resulting catalytic evaluations are given in the accompanying paper (6). Amidine, amido, and amino groups may be formed at residue 153 by alkylation. A variety of functional groups, including acetamidine (AAn), ethylamine (EAm), propylamine (PAm), acetamide (AAd), propylamide (PAd), and acetate (Ac) (6), may then be introduced at Sγ. In this manner both the distance and the type of potential interactions with the 1-carboxylate of the substrate may be varied.

Using the coordinates for R153C MDH with bound NAD, a model for each of the chemical modifications of Cys-153 was built. The newly generated side chains were evaluated with respect to their proximity to the 1-carboxyl of malate, which had been positioned in the active site from the theoretical model of eMDH·NAD·malate (*1cme*). Each new side chain was optimally oriented by rotation about dihedral angles to make the most favorable hydrogen bonding interactions with the substrate. The results are shown in Fig. 5 (*A–E*). Each new side chain, except for AAn, can be rotated to within ≤3.2 Å of the

TABLE III
Hydrogen bond interactions with ligands

		Subunit A	Subunit C	Subunit D
SO_4^{2-} A[a]	O1	Nδ2 Asn-119(3.05)	Nδ2 Asn-119(2.71)	Nδ2 Asn-119(2.81)
	O1		NH1 Arg-87(3.16)	NH1 Arg-87(3.21)
	O1		Nε2 His-177(3.22)	Nε2 His-177(2.77)
	O2	W355(2.73)	W475(3.24)	W535(2.63)
	O2			W536(2.90)
	O3	W346(2.55)	W476(2.57)	W534(2.71)
	O3			Nδ2 Asn-119(3.05)
	O4	NH1 Arg-87(2.98)	NH1 Arg-87(2.71)	NH1 Arg-87(2.56)
	O4	NH2 Arg-81(2.91)	NH2 Arg-81(2.75)	NH2 Arg-81(2.63)
	O4			W536(3.18)
SO_4^{2-} B[a]	O1	N Arg-87(2.86)	N Arg-87(3.07)	N Arg-87(2.74)
	O1	Nε Arg-87(3.07)		
	O1		W470(2.88)	
	O2		Oγ Ser-88(2.87)	
	O3	N Gly-179(3.08)	N Gly-179(2.90)	N Gly-179(2.64)
	O3	Nε Arg-87(3.14)	Nε Arg-87(2.80)	Nε Arg-87(2.89)
	O3			NH2 Arg-87(3.19)
Pyruvate[b]	O1		N Gly-179(3.77)	
	O2		N Gly-210(3.74)	
	O2		N Thr-211(3.85)	
	O3		Nε2 His-177(4.08)	
	O3		W478(3.61)	
Cytosol SO_4^{2-} [c]	O1	Nδ2 Asn-119(2.64)		
	O1	Nε2 His-177(2.84)		
	O2	Oγ1 Ser-225(2.92)		
	O3			
	O4	NH1 Arg-153(3.07)		
	O4	Nε2 His-177(3.18)		

[a] Sulfate ions in the R153C·NAD structure.
[b] Pyruvate from the R153C·NAD·pyruvate structure.
[c] Sulfate ion from the porcine cytoplasmic MDH structure (*4mdh*); residue numbers correspond to *E. coli*.
() Hydrogen bonding distance in angstroms.

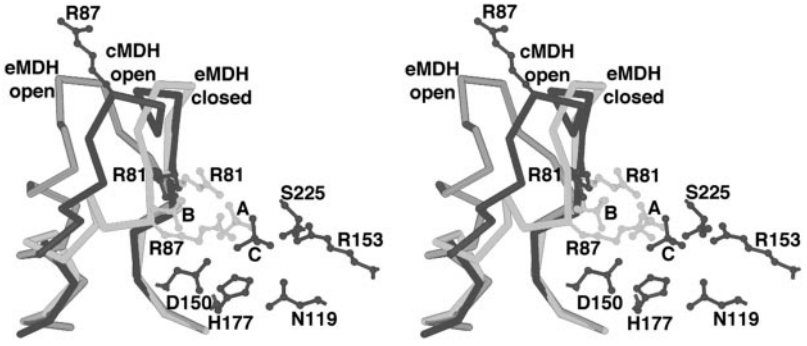

FIG. 3. **Comparison of sulfate positions in R153C eMDH and cytMDH.** A Cα trace of the active site loop from R153C eMDH·NAD·pyruvate (*gray*), R153C eMDH·NAD (*white*), and cytMDH·NAD (*dark gray*) (20). The three structures were superimposed using the LSQ options within O (11). The sulfate ion, labeled *C*, of cytMDH when compared with sulfate *A* of the R153C·NAD structure is translated ~2 Å farther into the active site. The hydrogen bonds between the sulfate and Ser-225 and Arg-153 provide the impetus for this translation.

1-carboxyl of malate. In the case of Ac, the proximity to the 1-carboxyl group would cause a charge-charge repulsion that may result in the side chain residing in an alternate rotamer position. The alternative rotamers could allow the Ac side chain to form hydrogen-bonding interactions with the side chain of Arg-205, the main chain nitrogens of 224 or 226, or solvent.

DISCUSSION

A fundamental question in enzymology bears upon how enzymes achieve substrate specificity. In general, the functional groups of a substrate are coordinated electrostatically or through hydrogen-bonding interactions with the atoms lining some portion of the active site. Additional binding stability may come from residues that are directly involved in catalysis, or result from a conformational change within the enzyme to promote catalysis. Several studies on MDH and a related enzyme, LDH, have identified a set of residues that are implicated in cofactor and substrate specificity and a conformational change of an active site loop involved in binding of the substrate.

For eMDH, three arginine residues (81, 87, and 153) in the substrate or anion binding site are positioned to both stabilize and orient the substrate for catalysis (Fig. 1). Prior studies have focused on the active site loop region, in particular Arg-81, and its contribution to substrate specificity (5, 18). From these studies the selectivity of di- *versus* monocarboxylic substrates does not appear to rely solely on interactions with Arg-81 (5) but changes in specificity can be obtained by the introduction of side chain analogues through chemical modification of the Cys-81 mutant (18). Therefore, Arg-81 plays a significant role in determining substrate specificity and may act in a concerted manner with other residues in the active site to achieve MDH's strict substrate specificity.

Within that context, what is the role of Arg-153 in substrate specificity? The two crystal structures of R153C eMDH reported here reveal the location of anions that are likely mimicking the positioning of substrates and/or inhibitors. The presence of substrate analogues in the active site allows a correlation to be drawn between the structural implications of the R153C mutant and the observed changes in the kinetic parameters. The binary and ternary complexes also demonstrate the two states of the active site loop (residues 79–91). Finally, the molecular modeling of the chemical modifications introduced at Cys-153 provides a basis for analyzing the ob-

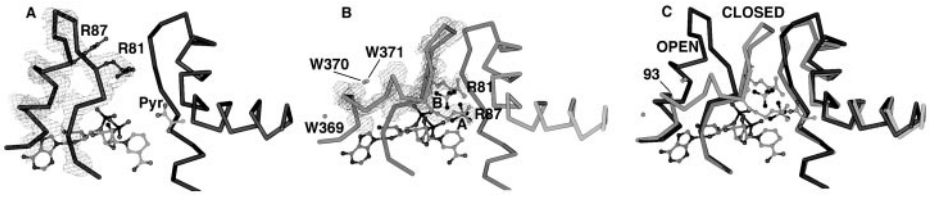

FIG. 4. **Comparing the open and closed conformations of the loop in R153C MDH.** *A*, Cα trace of the active site loop and adjacent loop in R153C·NAD·pyruvate subunit B shows how the side chains of Arg-81 and Arg-87 have moved out of the active site and are solvent-exposed. A $2|F_o| - |F_c|$ map, contoured at 1 σ, for the active site loop highlights the shift in its position and the extension of the α-helix to residue 86. *B*, Cα trace of the active site loop and adjacent loop in R153C·NAD with $2|F_o| - |F_c|$ electron density, contoured at 1 σ, encompassing the loop and the bent helix which directs Arg-87 into the active site. The three water molecules that bridge the $i+4$ hydrogen bonds are depicted by *gray spheres*. *C*, the R153C·NAD·pyruvate and R153C·NAD active site loops superimposed. At residue 93 the helix either bends, bringing Arg-81 and Arg-87 into the active site, or continues through residue 86 to expose the active site to solvent and, potentially, substrate.

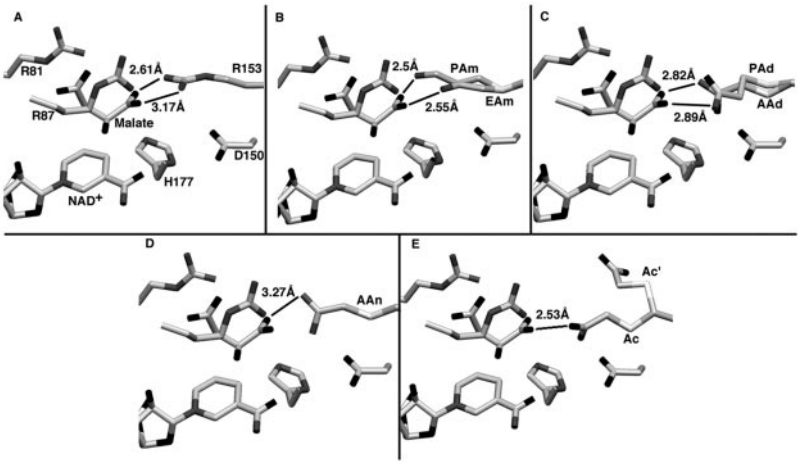

FIG. 5. **Models of the chemical modifications at R153C eMDH.** *A*, the active site of native eMDH shows the *theoretical* position of the malate with respect to the three coordinating arginines, Arg-81, Arg-87, and Arg-153. The potential hydrogen bonding interactions of the chemically modified cysteine at position 153, EAm and PAm (*B*), PAd and AAd (*C*), AAn (*D*), and Ac (*E*), are depicted by *black lines* drawn between acceptor and donor. An alternate rotamer is depicted for Ac, labeled *Ac′*, that has the side chain interacting with solvent.

served kinetic effects of the side chain analogues.

Implications of Substrate Analogue Position: Conformational Changes and Kinetic Effects—In the R153C·NAD·pyruvate structure (Fig. 4*A*), the active site loop is found in the *open* conformation. Comparing this open conformation to the closed form (NAD complex and *1emd*), the switch between the two conformations arises from a change in local secondary structure at residues 86–89 in the active site loop. The switch may be initiated by the coordination of Arg-81 and/or Arg-87 to an appropriate anion in the active site. To accommodate this interaction, the active site loop forms a bent 3_{10} helix. The bent helix is stabilized by solvent molecules bridging the $i+4$ hydrogen-bonding pattern within the helix. When residues in the loop do not form stabile interactions with the bound ligand, as in the NAD·pyruvate complex, residues 86–89 form a standard α-helix. The result is an open active site in which the loop is pulled back from the active site and exposed to solvent, explaining the greater disorder observed in this region.

The binding of a monocarboxylic inhibitor to the active site in the NAD·pyruvate ternary complex suggests that interactions with all of the active site arginines are not vital to filling the anion/substrate binding site. The pyruvate instead forms long hydrogen bonds to backbone amide groups, the catalytic histidine, and a water molecule (Table III). Nor is the closure of the active site loop necessary when compounds such as a monocarboxylic acid are bound. One could argue that the single negative charge on pyruvate is insufficient to interact optimally with the remaining cationic side chains around the active site. The crystallographic data further support these postulated weakened interactions by the incomplete occupancy within the crystal structure. The reduced affinity for pyruvate is also reflected in the 2-fold increase in K_i observed for this mutant. Native-like inhibition is regained when Cys-153 is chemically modified to a polar or charged group (6).

The structure of eMDH·NAD binary complex reveals a closed active site loop, the presence of an additional sulfate-binding site within the anion binding region, and a translation in the position of the conserved sulfate binding site. To explain the additional site, we hypothesize that the second anion is required to neutralize the charge-charge repulsion of Arg-81 and Arg-87 in the closed loop form. We propose that when the first sulfate binds in the anion pocket, the negative charge of this sulfate is coordinated by solvent molecules and one of the two remaining arginines in the active site loop. These two arginines are targeted due to the loss of the preferred site at Arg-153, as demonstrated by the cytMDH structure (20). The coordination of Arg-81 or Arg-87 to the sulfate may then induce the active site loop (residues 79–91) to adopt the closed conformation. The close proximity of Arg-81 and Arg-87 in the closed loop form would not be electrostatically favorable unless the positive side chains are neutralized with an additional negatively charged ligand. In the case of the binary complex of R153C eMDH, a second anion is present and appears to effectively balance the charges within the active site.

Sulfate A is translated ~2 Å toward the mouth of the active site when compared with the position of the cytMDH·NAD (*4mdh*) sulfate. In the cytMDH structure, the sulfate is coordinated by the guanidino group of Arg-153 and surrounding residues (Asn-119, His-177, and Ser-225; see Table III and Fig. 3). The interactions between Asn-119 and His-177 and the sulfate ion are conserved in the R153C structure, but additional electrostatic interactions are formed with the remaining arginines (Arg-81 and Arg-87). The added interactions with the active site loop drive the observed translation toward the opening of the cavity. This crystallographic observation lends support to the idea that the anion, attracted to the active site by the cationic side chains, may reside in multiple sites. Positioning of the anion is only critical when the compound is the substrate and must be aligned with the catalytic residues. To illustrate, if malate is translated the equivalent distance as

sulfate A, the 2-hydroxyl of malate would be 3.8–4 Å away from the Nϵ2 of the catalytic histidine. The result would be a less favorable orientation of the substrate with respect to the catalytic residues and cofactor for an efficient reaction. The approximately 7-fold decrease of k_{cat} for the reduction of oxaloacetate in the R153C mutant when compared with the native enzyme (6) is consistent with this hypothesis.

From this analysis, the coordination of the remaining arginines, Arg-81 and Arg-87, are sufficient, but not essential, for binding anions in the active site pocket. Interaction between the ligand bound in the active site and the active site loop arginines (Arg-81 and Arg-87) does appear necessary to signal closure of the active site loop. The effect of removing Arg-153 is most apparent in the marked decrease of catalysis that may, in part, be due to a change in the anion binding position as observed with sulfate A. Therefore, the role of Arg-153 in substrate specificity appears to be one of orienting the bound substrate into the *optimal* position for catalysis.

Structural Basis for Kinetic Effects in Chemically Modified R153C—The introduction of a cysteine into the eMDH active site has allowed a variety of functional groups to be incorporated through chemical modification and evaluated by steady state kinetics (6). To offer possible structural explanations for the kinetic results with the chemically modified R153C, molecular models for each of the modified side chains were built (Fig. 5). Adding coordinates to mimic the chemical modifications and observing the protein structure in terms of anion locations (derived here or in other crystallographic studies) forms the basis of the hypothetical models. Although there are a number of unforeseen difficulties in devising molecular models that are representative of dynamic solution structures, the crystallographic coordinates provide a clear starting point for developing a direct link to the catalytic reaction. It is evident from the models that all but AAn (due to the shorter side chain) and Ac (due to charge repulsion) are capable of making good, ($\leq$3.2-Å) hydrogen bonding interactions with the malate positioned in the active site.

Even though the AAn-modified enzyme could not make close contacts with the dicarboxylic acid substrate, it does provide the most effective mimic of the arginine side chain. The 2.5- and 5-fold decrease in K_m over the native and mutant enzyme for OAA reduction, respectively, and the 5-fold reduction of k_{cat}/K_m suggests that the unnatural side chain does not significantly alter the interactions with substrate. However, the incorporation of the AAn side chain is insufficient to completely regain wild type activity (6). The inability to totally recover wild type catalytic properties with the AAn modified Cys-153 enzyme may be due to the guanidino group foreshortened by one carbon. The shortened side chain would result in a less than optimal alignment of the substrate's 2-hydroxyl/keto with the catalytic histidine and nicotinamide ring.

The addition of a side chain homologue such as a PAd or PAm group, which is able to coordinate the 1-carboxyl of the substrate, improves k_{cat} by 1.7–2.1-fold over that of unmodified R153C for OAA reduction. Neither homologue can recover wild-type catalytic activity, even though they provide a positively charged side chain. One might speculate that electrostatic coordination of only one oxygen of the substrate's 1-carboxylate is not sufficient to stabilize the orientation of the substrate and the resulting minor misalignment is felt throughout the catalytic process.

Consistent with the crystallographic analysis, the molecular models suggest that it is a well balanced combination of position, charge, and the bidentate nature of the guanidino group at position 153 that orients the substrate for the most efficient catalytic turnover and contributes to substrate specificity.

Finally, the combined crystallographic and model building data have provided a new insight into substrate binding in the MDHs. The connected volume of anionic compounds found in the various crystallographic studies of the MDHs was shown in Fig. 1. Noteworthy is the fact that with the flexibility of Arg-153, Arg-81, and Arg-87, and potential main chain conformational changes that can occur in the loop region, the binding location of an anionic compound may be quite varied. Negative charges may be easily accommodated in a variety of active site locations, as is evident in MDH's ability to bind a single sulfate to a 6-carbon tricarboxylic acid. Specificity appears, therefore, to be derived not from binding alone but from the location of the catalytic clusters, His-177 and Asp-150, the position of the nicotinamide ring of the cofactor, and the ability of the enzyme interactions, most notably by the active site arginines, to orient the substrate for productive catalysis.

Acknowledgements—We acknowledge Judy Bratt (University of Minnesota, Minneapolis, MN) for crystal setup. We are deeply grateful to Ed Hoeffner for maintenance of the University of Minnesota x-ray equipment and computational support. The Minnesota Supercomputing Institute generously supported computations necessary for the x-ray crystallographic and model building experiments.

REFERENCES

1. Hall, M. D., and Banaszak, L. J. (1993) *J. Mol. Biol.* **232,** 213–222
2. Chapman, A. D. M., Cortes, A., Dafforn, T. R., Clarke, A. R., and Brady, R. L. (1999) *J. Mol. Biol.* **285,** 703–712
3. Birktoft, J. J., and Banaszak, L. J. (1983) *J. Biol. Chem.* **258,** 472–482
4. Wilks, H. M., Hart, K. W., Feeney, R., Dunn, C. R., Muirhead, H., Chia, W. N., Barstow, D. A., Atkinson, T., Clarke, A. R., and Holbrook, J. J. (1988) *Science* **242,** 1541–1544
5. Nicholls, D., Miller, J., Scawen, M., Clarke, A. R., Holbrook, J. J., Atkinson, T., and Goward, C. (1992) *Biochem. Biophys. Res. Commun.* **189,** 1057–1062
6. Wright, S. K., and Viola, R. E. (2001) *J. Biol. Chem.* **276,** 31151–31155
7. Hall, M., Levitt, D., McAlister-Henn, L., and Banaszak, L. J. (1991) *J. Mol. Biol.* **220,** 551–553
8. Navaza, J. (1994) *Acta Crystallogr. Sect. A* **50,** 157–163
9. Castellano, E., Oliva, G., and Navaza, J. (1992) *J. Appl. Crystallogr.* **25,** 281–284
10. Brunger, A. T., Adams, P. D., Clore, G. M., Delano, W. L., Gros, P., Grossekunstleve, R. W., Jiang, J. S., Kuszewski, J., Nilges, M., Pannu, N. S., Read, R. J., Rice, L. M., Simonson, T., and Warren, G. L. (1998) *Acta Crystallogr. Sect. D Biol. Crystallogr.* **54,** 905–921
11. Jones, T., Zou, J., Cowan, S., and Kjeldgaard, M. (1991) *Acta Crystallogr. Sect. A* **47,** 110–119
12. Kleywegt, G. J., and Jones, T. A. (1998) *Acta Crystallogr. Sect. D Biol. Crystallogr.* **54,** 1119–1131
13. Vriend, G. (1990) *J. Mol. Graph.* **8,** 52–56
14. Rodriguez, R., Chinea, G., Lopez, N., Pons, T., and Vriend, G. (1998) *Comput. Appl. Biosci.* **14,** 523–528
15. Laskowski, R., MacArthur, M., Moss, D., and Thornton, J. M. (1993) *J. Appl. Crystallogr.* **26,** 283–291
16. Otwinowski, Z., and Minor, W. (1997) *Methods Enzymol.* **276,** 307–326
17. Evans, S. V. (1993) *J. Mol. Graph.* **11,** 134–138
18. Wright, S. K., Kish, M. M., and Viola, R. E. (2000) *J. Biol. Chem.* **275,** 31689–31694
19. Hall, M., Levitt, D., and Banaszak, L. J. (1992) *J. Mol. Biol.* **226,** 867–882
20. Birktoft, J. J., Rhodes, G., and Banaszak, L. J. (1989) *Biochemistry* **28,** 6065–6081
21. Kabsch, W., and Sander, C. (1983) *Biopolymers* **22,** 2577–2637